THE JOURNAL OF PHYSICAL CHEMISTRY LETTERS
A JOURNAL OF THE AMERICAN CHEMICAL SOCIETY

pubs.acs.org/JPCL

Letter

High-Pressure Synthesis and Characterization of the Novel Potassium Superhydride KH_9

Tomas Marqueño, Israel Osmond, Mikhail A. Kuzovnikov, Hannah A. Shuttleworth, Andreas Hermann, Ross T. Howie, and Miriam Peña-Alvarez*

Cite This: J. Phys. Chem. Lett. 2025, 16, 9701−9707

Read Online

ACCESS | Metrics & More | Article Recommendations | Supporting Information

ABSTRACT: Through high-pressure diamond anvil cell experiments, we report the synthesis of two novel potassium superhydrides (KH_9-I and KH_9-II) and investigate their structural and vibrational properties via synchrotron X-ray powder diffraction and Raman spectroscopy, complemented by density functional theory (DFT) calculations. Above 17 GPa at room temperature, KH-II and H_2 react to form KH_9-I; this reaction can be accelerated with temperature. KH_9-I possesses a face-centered-cubic (*fcc*) potassium sublattice with a slight rhombohedral distortion (space group *R*3*m*). Compression above 78 GPa converts KH_9-I to another polymorph, KH_9-II, which adopts a primitive simple hexagonal potassium sublattice (space group *P*6/*mmm*) and remains stable up to at least 100 GPa. Both KH_9 polymorphs exhibit ionic character, comprising K^+ and H^- ions, along with quasi-molecular H_2 units, resulting in rich Raman activity.

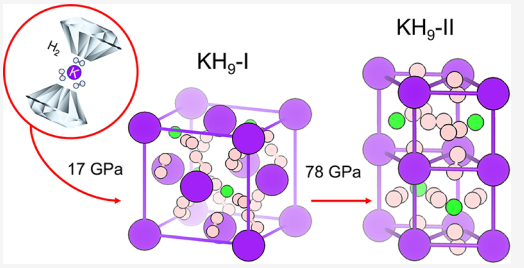

In recent decades, the high-pressure synthesis of binary metal−hydrogen systems have attracted significant attention due to their capacity to produce hydrogen-rich materials (polyhydrides) with unconventional properties, including high-temperature superconductivity, such as LaH_{10}[1] and H_3S.[2] In particular, alkali metal polyhydrides have garnered interest due to their predicted low formation pressure, high hydrogen content, novel hydrogen motifs[3−6] and more recently, potential high-temperature superconductivity.[7−9]

Theoretical predictions of alkali superhydrides initially prompted experimental exploration of the Li−H system at high pressures.[7] Infrared (IR) spectroscopic studies suggested the formation of LiH_2 and LiH_6 above 130 GPa as disproportionation products of LiH.[10] Subsequently, the synthesis of NaH_3 (*Cmcm*) was reported at pressures above 30 GPa.[11,12] The formation of NaH_7 was claimed;[11] however, it has been alleged to be a misinterpretation due to sample contamination.[12,13] Rubidium and cesium superhydrides at high pressures have been reported from decomposition products of quaternary compounds $RbNH_2BH_3$ and $CsNH_2BH_3$.[14] In a more recent work, the rubidium superhydrides, RbH_5 and RbH_9, were thoroughly studied from pure samples of Rb and H_2.[15] RbH_9 exists in two forms: RbH_9-I with slightly distorted hexagonal close-packed (*hcp*) Rb sublattice, stable between 8.7 and 15 GPa, and RbH_9-II, with primitive simple hexagonal (*sh*) Rb sublattice, stable between 15 and 87 GPa. All these hydrides host alkaline cations (M^+), H^- anions, and quasi-molecular H_2 units. Here, "quasi-molecular H_2" refers to H_2 molecules that are doped by charges from the host lattice and/or confined within small interstitial sites, which alters the bond order of the H_2 units.[16,17]

The only alkali metal hydride system yet to be experimentally explored is the potassium−hydrogen system. Theoretical calculations indicate that potassium has the potential to form polyhydrides at pressures as low as 3 GPa.[4] At pressures of 30 GPa, the only two potassium polyhydrides predicted to lie on the convex hull are *Cmcm*-KH_5 and KH_9.[4] At even higher pressures, other stoichiometries such as *Imm*2-KH_{11} (50 GPa)[18] and *C*2/*m*-KH_8 (at 100 GPa)[4] become thermodynamically favorable. More recently, two polymorphs of KH_{10} (space groups *C*2/*m*[8] and *Immm*[18]) were predicted to be dynamically stable at 100 GPa, both of which were proposed to exhibit high-temperature superconductivity, with T_c ranging from 105 to 157 K at 100 GPa.[8,18] A different work predicted that at pressures above 400 GPa, KH_{20} and KH_{30} would become stable, while exhibiting superconductivity near room temperature.[19] Despite these wide ranging predictions, potassium monohydride, KH, is the only one experimentally studied. KH adopts a NaCl-type structure, KH-I, which converts into CsCl-type KH-II upon compression at 4 GPa and is stable in an inert medium up to at least 25 GPa.[20]

Received: July 1, 2025
Revised: July 29, 2025
Accepted: August 1, 2025
Published: September 9, 2025

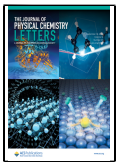

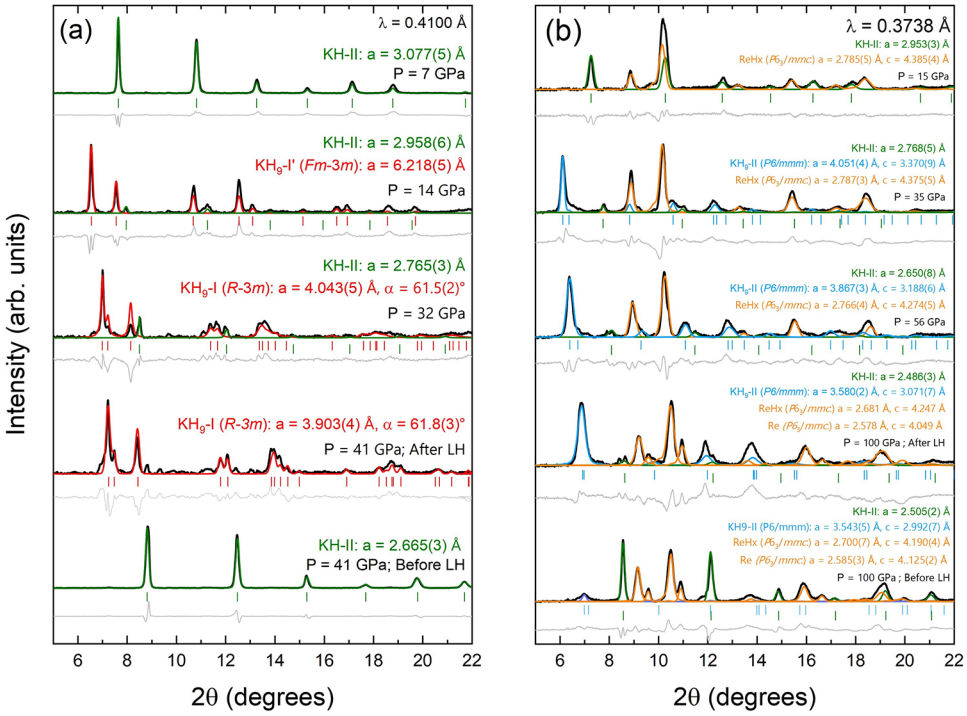

Figure 1. Selected XRD patterns collected during decompression after laser heating at (a) 41 and (b) 100 GPa. Experimental data are shown as black solid curves. Red, blue, green, and orange solid curves represent the calculated Rietveld refinements with contributions from KH_9-I/-I′, KH_9-II, KH-II, and ReH_x+Re phases, respectively. Gray curves represent the refinement residuals. Vertical ticks indicate the calculated positions of the Bragg reflections for each phase (except ReH_x+Re).

In this work, we synthesize KH_9 through a series of diamond anvil cell (DAC) experiments at pressures between 17 and 100 GPa. We characterize KH_9 using synchrotron X-ray diffraction (XRD) and Raman spectroscopy, combined with density functional theory (DFT) and molecular dynamics (MD) calculations. Two KH_9 polymorphs are identified: KH_9-I, which features a potassium sublattice adopting a distorted face-centered cubic (*fcc*) structure consistent with rhombohedral symmetry ($R\bar{3}m$); and KH_9-II, which exhibits a primitive hexagonal sublattice ($P6/mmm$). KH_9-I forms when KH-II is compressed above 17 GPa in the presence of H_2; laser heating significantly accelerates the reaction. Upon decompression below 15 GPa, the potassium sublattice of KH_9-I progressively transforms into a symmetric *fcc* structure (KH_9-I′). This KH_9-I′ remains stable down to approximately 13 GPa, before decomposing into KH-II and H_2. KH_9-I remains stable upon compression up to 78 GPa. Laser heating between 78 and 100 GPa leads to the formation of KH_9-II, which partially converts back to KH_9-I upon decompression to 35 GPa. Both KH_9 polymorphs display Raman features consistent with quasi-molecular hydrogen, in good agreement with our DFT calculations.

Potassium metal (99.75%, Alfa Aesar) was loaded into a DAC in an inert argon atmosphere. The sample chamber was hermetically sealed, and the DAC was then transferred to a high-pressure-loading apparatus, where hydrogen gas (99.9995% purity, BOC) was loaded at a pressure of 0.2 GPa. Hydrogen was supplied in excess, and served both as a reactant and a pressure transmitting medium. Pressure was determined either by the equation of state of gold during XRD measurements[21] or by Raman spectroscopy via the Raman shift of the intramolecular H−H stretching mode.[22] Further experimental details are given in the Supporting Information.

Exposure to hydrogen during loading caused potassium metal to convert into KH-I (*fcc*) as evidenced by the partial transparency of the sample (Supporting Information Figure S1a). Subsequent X-ray diffraction measurements confirmed complete transformation of the sample, with no detectable traces of the K precursor, see bottom curve in Figure 1a. Consistent with prior work, the structural transition from KH-I (*fcc*) to KH-II (*sc*) was observed at 5 GPa.[20] Previous studies on KH were limited to pressures below 25 GPa.[20] Our study demonstrates that KH-II persists up to 110 GPa, revealing no evidence of any further phase transitions. The fit of the $V(P)$ data for KH-II with the Birch−Murnaghan equation of state[23] is shown by the dashed green curve in Figure 2a. The obtained EOS parameters for KH-II are shown in Table S2.

Upon compression of KH-II in an H_2 media at pressures above ∼17 GPa, we observe new features in the Raman spectra, which we attribute to the formation of a new polyhydride, as shown in Figure S2. As this reaction can take place without laser heating, the possibility of methane contamination can be excluded. Furthermore, laser heating to temperatures exceeding 1200 K,[24] accelerates the reaction (Figures S1b and S2a). The synthesis of a new compound is further evidenced by distinct changes in the X-ray diffraction pattern, as shown in Figure 1a. Rietveld refinement of the data reveals that the potassium sublattice of the reaction product adopts an *fcc* structure with a minor rhombohedral distortion ($R\bar{3}m$) with lattice parameters a = 3.903 Å and α = 61.8° (compared to α = 60° for an undistorted *fcc* lattice). The reaction is accompanied by a substantial volume increase of the solid phase: from 19.4 to 43.7 Å^3 per K atom at 41 GPa. Because the total volume effect should be negative for the formation reaction KH-II + $[(x - 1)/2]H_2 \rightarrow KH_x$, the hydrogen content of the new hydride, KH_x, is no less than H/

https://doi.org/10.1021/acs.jpclett.5c02024
J. Phys. Chem. Lett. 2025, 16, 9701−9707

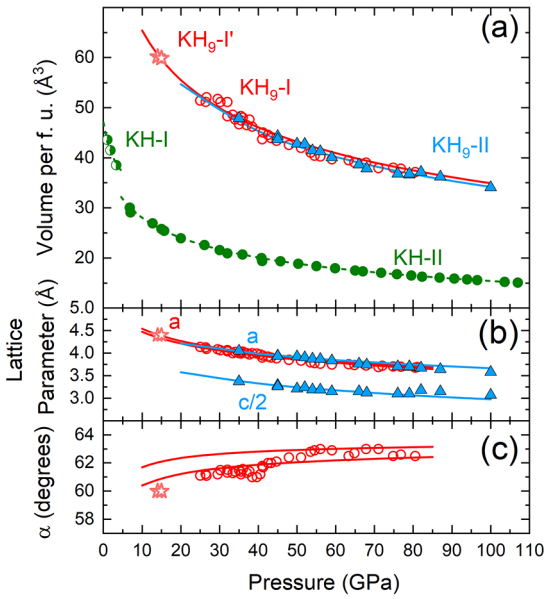

Figure 2. (a) Pressure dependence of the volume per formula unit (f.u.) of KH_9 and KH. Data for KH_9-I′/-I and -II are represented with red empty stars/circles and blue triangles, respectively. Red and blue solid curves stand for our DFT-calculated values for KH_9-I (*Cm*) and -II (*Cccm*), respectively. Green symbols represent KH-II data. Green half-filled symbols represent the KH-I data. The green dashed curve represents a Birch−Murnaghan EOS fit to the KH data with the parameters listed in Table S2. (b, c) Pressure evolution of the lattice parameters of KH_9-I and -II.

$K > 1 + 2\Delta V/V(H_2) = 1 + 2(43.7 - 19.4)/6.74 = 8.2$, using $V(H_2) = 6.74$ Å^3/H_2 at 41 GPa,[25] supporting the assignment of the stoichiometry as KH_9-I. Upon decompression, the rhombohedral ($R\bar{3}m$) distortion progressively disappears, and the potassium sublattice transitions to a symmetric *fcc* structure at ∼14 GPa, which we presently call KH_9-I′, with lattice parameter $a = 6.218(5)$ Å, as shown in Figure 1a. At the subsequent decompression step, no diffraction features attributable to KH_9-I/-I′ can be detected, indicating that the compound decomposes into KH-II and H_2 between 14 and 7 GPa; see the top pattern in Figure 1a. The decomposition is also observed in independent Raman experiments, which show that KH_9-I starts decomposing at 13 GPa (Figure S2a).

On room temperature compression alone, we observe that above 78 GPa, KH_9-I transforms into another polymorph, KH_9-II, evidenced through Raman spectroscopy (Figure S2b). X-ray diffraction measurements show that this reaction is sluggish, with only a few weak reflections that we attribute to KH_9-II observed in the X-ray diffraction pattern (see the bottom pattern in Figure 1b). Laser heating at 100 GPa induced a noticeable volume expansion of the KH phase (Figure S3a,b), indicative of further hydrogen uptake. XRD patterns collected after heating suggest that most of the sample transformed into the new polyhydride KH_9-II. Rietveld refinement shown in Figure 1b indicates that KH_9-II adopts a primitive simple hexagonal potassium sublattice. The relative intensities of the new diffraction peaks suggest a preferred orientation of KH_9-II crystallites along the *c*-axis, consistent with typical growth in hexagonal systems. KH_9-II is observed on decompression down to 35 GPa (Figure 1b); at the subsequent decompression step, at 10 GPa, the sample consists entirely of KH-II and H_2, indicating that KH_9-II had decomposed into its initial constituents.

Figure 2a shows the pressure evolution of the volume per K atom for the newly synthesized KH_9 polymorphs (see Table S2 for equation of state parameters), as well as for KH phases I and II. Panels b and c of Figure 2 show the pressure dependence of the lattice parameters for the KH_9 phases, as extracted from Rietveld refinements. The *a*-axis values for both KH_9-I and KH_9-II overlap, as expected, since the two structures are related by a relative shift of consecutive hexagonal planes. In KH_9-I, the α angle becomes larger with increasing pressure, indicating that compression enhances the rhombohedral distortion. This enables a comparison between the DFT and the experimental structures, because DFT is a lower symmetry structure. This lower symmetry structure needs to be transformed into the coordinate system of the higher symmetry experimental one (see Supporting Information). In the case of KH_9-I, the transformation from a monoclinic structure into rhombohedral axes ($Cm \rightarrow R\bar{3}m$) leads to two different values of *a* and α, as shown in Figure 2b,c. The rhombohedral α angle progressively increases with pressure up to ∼45 GPa. Beyond this pressure, the angle remains approximately constant at around ∼62.5°.

As shown in Figure 3a,b, both KH_9-I and -II present intense Raman features in two distinct spectral regions: low

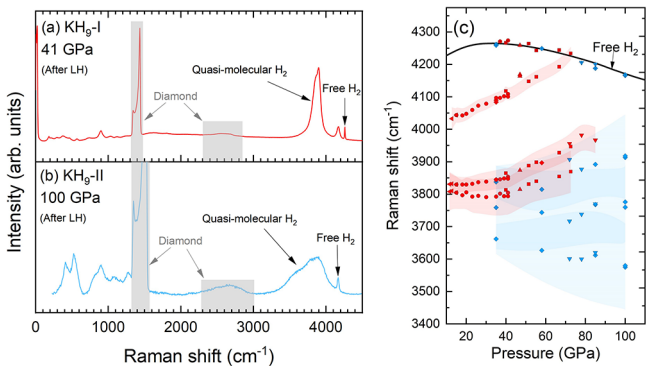

Figure 3. Raman spectra of (a) KH_9-I after laser heating at 41 GPa (red curve) and (b) KH_9-II after laser heating at 100 GPa (blue curve). The shaded areas in gray indicate the Raman active modes of diamond. (c) Pressure dependence of the vibron frequencies for both KH_9-I and -II (red and blue symbols, respectively). Different symbol types correspond to different experiments. Shaded areas represent the error bars (peak widths) of the data. Frequencies of excess H_2 are shown as crossed symbols, while literature data from pure H_2 are represented by a black curve.[22]

frequencies ($\Delta\nu < 1300$ cm^{-1}) and high frequencies ($\Delta\nu > 3500$ cm^{-1}). The simulated Raman spectra for both KH_9 polymorphs at similar pressures are shown in Figure S4. DFT calculations indicate that the low-frequency modes correspond to librational motions, while the high-frequency modes are associated with the stretching vibrations of quasi-molecular H_2 (Figures S5 and S6).[12] Second-derivative analysis reveals that the high-frequency bands can be deconvoluted into three distinct contributions, corresponding to the stretching modes of quasi-molecular H_2 within KH_9 (Figure S7a,b). In KH_9-I, two broad and intense peaks are centered around 3800 cm^{-1}, with a third weaker peak upshifted by about 200 cm^{-1}. In contrast, KH_9-II shows three broader peaks clustered at lower frequencies, around 3700 cm^{-1}. Most of these alkali polyhydrides with quasi-molecular H_2 units, exhibit strong Raman activity in the 3000−4200 cm^{-1} spectral region as

https://doi.org/10.1021/acs.jpclett.5c02024
J. Phys. Chem. Lett. 2025, 16, 9701−9707

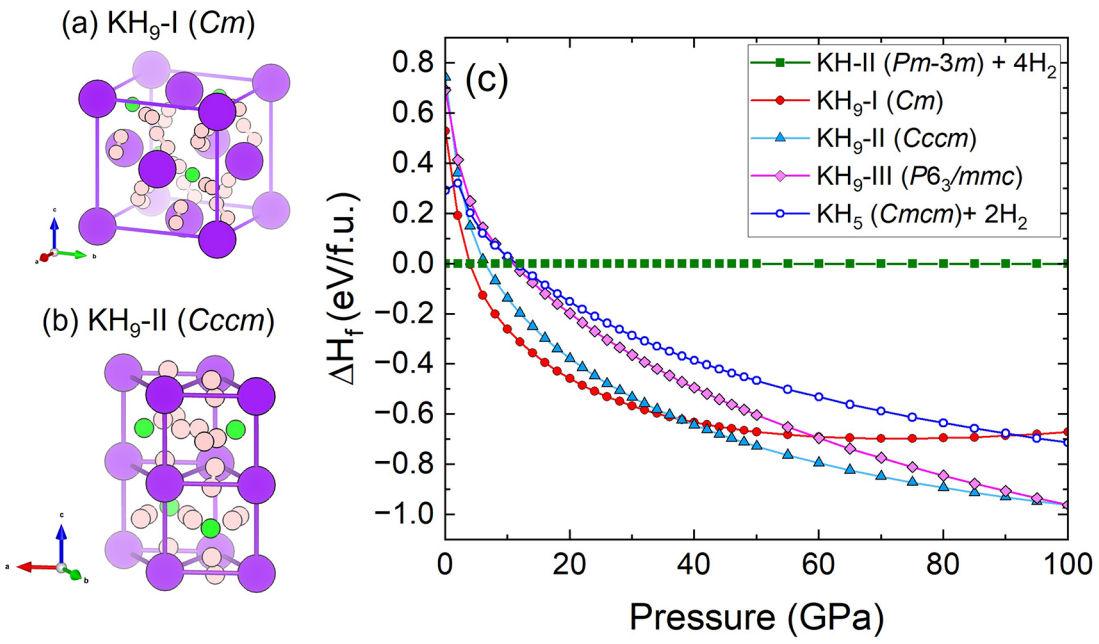

Figure 4. (a, b) Predicted crystal structures of KH_9-I (in *fcc* axes) and KH_9-II (hexagonal axes), respectively. Purple, pink, and green spheres represent K^+ cations, quasi-molecular H_2 units, and anionic H^- species, respectively. (c) Calculated enthalpy curves for KH_9 and KH_5 phases, relative to their initial constituents, KH-II + H_2.

well.[12,26] The evolution of the Raman shift of these H−H stretching modes from the hosted quasi-molecular H_2 units is an indicator of the efficiency in the chemical precompression of H_2; the greater the down shift of this mode is compared to that of pure H_2, the more efficient the chemical precompression is.[16] The pressure dependence of the vibron frequencies for both KH_9-I and -II is presented in Figure 3c. For KH_9-I, the low-frequency contributions to the stretching H−H vibron initially down shift upon compression up to 40 GPa, at which point they change their slope to up shift with compression. The high-frequency vibron of KH_9-I exhibits a positive slope at any pressure, eventually overlapping with pure hydrogen vibron at about 80 GPa. These results are in agreement with DFT predictions for KH_9-I, Figure S8a. In contrast, for KH_9-II, only the highest-frequency vibron exhibits a clear hardening with increasing pressure. The effect of pressure on the other two vibrons in KH_9-II is primarily observed as peak broadening with no significant shifting. This behavior is not well captured by DFT calculations, which, despite an initial down shift with respect to the KH_9-I vibrons, predict a positive pressure dependence for all high-frequency modes in KH_9-II (see Figure S8a). Thus, it is possible that DFT calculations underestimate the interactions of quasi-molecular hydrogen for denser phases as in KH_9-II. At the same time, the low-frequency modes of KH_9, all of the observed modes harden upon compression, as shown in Figure S8b.

Hooper and Zurek[4] predicted that KH_9 (with an unspecified space group) is the most stable stoichiometry together with KH_5 (*Cmcm*) between 5 and 30 GPa. Semenok et al.[18] later predicted that KH_9 (*Cm*), KH_{11} (*Imm*2), KH_5 (*Cmcm*), and KH-II lie on the convex hull at 50 GPa. We performed DFT calculations for various stoichiometries in the K−H system at 10−100 GPa, as shown in Figure S9a,b (KH_5 and KH_{7-11}), observing that KH_9 lies on the convex hull at all examined pressures. KH_5, as previously predicted, also lies on the convex hull at 50 GPa.[4,18] The predicted KH_5 (*Cmcm*) (Figure S10a) is isomorphic to the previously reported RbH_5-I.[26] However, in equilibrium in a hydrogen-rich environment only KH_9 is predicted to form, in agreement with our experimental observations (KH_5 should form if the KH:H_2 ratio in the sample were less than 1:4).

The potassium sublattice of *Cm*-KH_9,[18] is remarkably similar to the one presently observed for KH_9-I. The metal sublattice of KH_9-II is isomorphic to RbH_9-II,[26] for which a full crystal structure model with a *Cccm* space group was considered. Consequently, in our present DFT calculations we take the *Cm*[18] and *Cccm*[26] as structural models for KH_9-I and KH_9-II, respectively, Figure 4a,b. Figure 2 shows the pressure evolution of the volumes calculated with DFT (a) and the lattice parameters (b, c), indicated by the red and blue curves for KH_9-I and KH_9-II, respectively, presenting an excellent agreement with the experimental results (see Tables S3−S5 for parameters and transformation matrices). According to our calculations of enthalpy, KH_9-I (*Cm*) is thermodynamically stable above 5 GPa with respect to KH+4H_2 (Figure 4c). Above 38 GPa, KH_9-II (*Cccm*) becomes energetically more favorable than KH_9-I (Figure 4). In addition, above 100 GPa, KH_9-III ($P6_3/mmc$) with a primitive simple hexagonal K sublattice, similar to KH_9-II, becomes more stable than KH_9-II (Figure 4c).

All KH_9-I, -II, and -III are found to be dynamically stable in the calculations; see Figure S11 for the phonon dispersions and Figure S4 for Raman. Including vibrational entropies to obtain harmonic free energies has a very small impact on the relative stabilities of KH_9-I/-II/-III, as shown in Figure S9c. To further account for possible thermal motion effects, ab initio molecular dynamics (MD) simulations were performed using KH_9-I (*Cm*) as the starting structure. The simulated XRD patterns at 40 GPa (see Figure S12) show that the K sublattice of KH_9-I evolves toward the rhombohedral structure ($R\bar{3}m$), which was observed in our XRD and Raman experiments. MD calculations also suggest that the degree of rhombohedral distortion decreases at lower pressures (see Figure S13), which

https://doi.org/10.1021/acs.jpclett.5c02024
J. Phys. Chem. Lett. 2025, 16, 9701−9707

may ultimately result in transitioning to the symmetric *fcc* K sublattice, as was observed experimentally.

Calculations show that both KH_9 phases are semiconductors over the entire pressure range studied here. See Figures S14–S16 for electronic density of states (DOS) and band gap evolution with pressure. At 100 GPa, the DFT band gaps are 1.47 and 1.16 eV for KH_9-I (*Cm*) and -II (*Cccm*), respectively (likely underestimated). A QTAIM partial charge analysis[27] confirms their mixed molecular and ionic character: in the 10–100 GPa pressure range, K cations have a partial charge of between +0.81 and +0.60, isolated H^- anions have a partial charge of between −0.54 and −0.39, and H_2 molecules have a partial charge of less than −0.03 that does not considerably change withing the explored pressure range (see Figure S16). Plots of the electron localization function (ELF) in Figure S16 corroborate this picture. The lack of charge transfer to the H_2 molecules aligns with the spectral observations for the H–H stretching vibrons of both polymorphs, which either harden or show negligible shifts with pressure (Figure 3c).[16]

Among alkali metal–hydrogen system under pressure, a polyhydride with a hydrogen to metal ratio of nine has only been observed in the Rb–H system.[26] In particular, while RbH_9-I and KH_9-I are structurally distinct, RbH_9-II and KH_9-II are isomorphic. The key difference between these phases lies in their pressure ranges of stability: RbH_9-II forms at pressures as low as 22 GPa, whereas the synthesis of KH_9-II requires pressures above 78 GPa. In contrast to the Rb–H system, where a lower hydride, RbH_5, can be synthesized at hydrogen pressures above 87 GPa, no intermediate hydrides with $1 < H/K < 9$ were observed in the K–H system over the pressure range studied, which includes more than 10 loadings with various K/H_2 ratios.

It is generally believed that the thermodynamic equilibrium pressure in the metal–hydrogen systems lies closer to the decomposition pressure than to the midpoint between formation and decomposition.[28] Assuming that the equilibrium and decomposition pressures are identical, we conclude that the minimum pressures at which superhydrides become stable in the K–H and Rb–H systems are similar: 13 GPa for KH_9 vs 8.7 GPa for RbH_9. The sightly lower value for RbH_9 is likely due to the larger ionic radius of the Rb^+ cation. This is a common trend among alkali and alkaline-earth metal polyhydrides, and it has been particularly observed for the alkaline-earth metal tetrahydrides.[16]

Gravimetric hydrogen storage capacity is a crucial concept in hydrogen-based technologies, as it tells us how efficiently a material can store hydrogen by weight. This is essential for energy storage and transportation applications, such as fuel cell vehicles and aerospace.[29,30] KH_9 has the highest reversible gravimetric hydrogen storage capacity (17 wt %) among all known binary hydrides, excluding van der Waals compounds $(CH_4)_2(H_2)_{17}$,[13] $H_2O(H_2)_2$,[31] and $HI(H_2)_{13}$.[32] This is more than 3 times the current target for hydrogen storage for light-duty fuel cell vehicles set by the U.S. Department of Energy (≥5.5 wt % in 2025).[33]

Despite numerous theoretical predictions of stable superconducting alkali-metal polyhydrides,[8] none of these phases have been experimentally observed.[10−12,14,26] The lack of superconductivity in the reported alkali metal polyhydrides is related to the fact that most high-pressure experimental studies show they host quasi-molecular hydrogen and not the atomic hydrogen lattice that is typically characteristic of superconducting polyhydrides.[10−12,14,26] Although DFT predicts that quasi-molecular H_2 can support high-T_c superconductivity,[34,35] experimental verification remains challenging.[16,36] As an alternative approach in the synthesis and characterization of hydrogen-based superconductors, theoretical studies have proposed exploring ternary hydrides combining alkali metals with other elements, such as different alkali metals,[37] transition metals[38,39] or p-block elements.[40,41] However, there remains limited experimental evidence for superconducting behavior in such systems.[42−46]

Conclusions: This study concludes the systematic investigation of alkali hydrides under high pressure, completing the series with the previously unexplored potassium hydride. Potassium nonahydride, KH_9, was synthesized from KH and H_2 at pressures between 17 and 100 GPa using diamond anvil cells. XRD experiments confirm the existence of two distinct KH_9 polymorphs. KH_9-I features a primitive rhombohedral potassium sublattice with space group $R\bar{3}m$, which symmetrizes into a *fcc* structure upon decompression below 15 GPa, KH_9-I′. Further pressure release leads to decomposition into KH-II and H_2 near 13 GPa. KH_9-II, characterized by a primitive simple hexagonal potassium sublattice (*P6/mmm*), was obtained by laser heating a mixture of KH-II and excess H_2 at 100 GPa, and remains stable down to at least 35 GPa, based on XRD measurements. Raman spectroscopy reveals that KH_9-I transforms into KH_9-II upon compression around 78 GPa, while partial reversion to KH_9-I occurs upon decompression below ∼35 GPa. Both KH_9-I and KH_9-II host quasi-molecular H_2 units, as evidenced by strong Raman bands above 3500 cm^{-1}.

■ ASSOCIATED CONTENT

Supporting Information

The Supporting Information file contains the following information: (i) a table summarizing key details of the beamlines used for our XRD experiments, (ii) the simulation details, (iii) additional experimental data, including XRD patterns, Raman spectra and sample images; and (iv) the results of our MD simulations. The Supporting Information is available free of charge at https://pubs.acs.org/doi/10.1021/acs.jpclett.5c02024.

(PDF)

■ AUTHOR INFORMATION

Corresponding Author

Miriam Peña-Alvarez − *Center for Science at Extreme Conditions (CSEC) and the School of Physics and Astronomy, The University of Edinburgh, EH9 3JZ Edinburgh, United Kingdom;* orcid.org/0000-0001-7056-7158; Email: miriam.pena.alvarez@ed.ac.uk

Authors

Tomas Marqueño − *Center for Science at Extreme Conditions (CSEC) and the School of Physics and Astronomy, The University of Edinburgh, EH9 3JZ Edinburgh, United Kingdom;* orcid.org/0000-0001-5371-1082

Israel Osmond − *Center for Science at Extreme Conditions (CSEC) and the School of Physics and Astronomy, The University of Edinburgh, EH9 3JZ Edinburgh, United Kingdom;* orcid.org/0000-0001-8756-8501

Mikhail A. Kuzovnikov − *Center for Science at Extreme Conditions (CSEC) and the School of Physics and Astronomy, The University of Edinburgh, EH9 3JZ*

https://doi.org/10.1021/acs.jpclett.5c02024
J. Phys. Chem. Lett. 2025, 16, 9701−9707

Edinburgh, United Kingdom; orcid.org/0000-0003-4030-4861

Hannah A. Shuttleworth − *Center for Science at Extreme Conditions (CSEC) and the School of Physics and Astronomy, The University of Edinburgh, EH9 3JZ Edinburgh, United Kingdom;* orcid.org/0000-0002-5113-1575

Andreas Hermann − *Center for Science at Extreme Conditions (CSEC) and the School of Physics and Astronomy, The University of Edinburgh, EH9 3JZ Edinburgh, United Kingdom;* orcid.org/0000-0002-8971-3933

Ross T. Howie − *Center for Science at Extreme Conditions (CSEC) and the School of Physics and Astronomy, The University of Edinburgh, EH9 3JZ Edinburgh, United Kingdom; Centre for High Pressure Science and Technology Advanced Research, Pudong, Shanghai 201203, People's Republic of China;* orcid.org/0000-0002-7013-8211

Complete contact information is available at: https://pubs.acs.org/10.1021/acs.jpclett.5c02024

Notes

The authors declare no competing financial interest.

■ ACKNOWLEDGMENTS

This work was supported by the UKRI Future Leaders Fellowship Mrc-Mr/T043733/1 and by the European Research Council (ERC) under the European Union's Horizon 2020 research and innovation program (Grant Agreement no. 948895, MetElOne). The authors thank Prof. M. McMahon for providing access to the glovebox in his laboratory for potassium sample loading. We acknowledge DESY (Hamburg, Germany), a member of the Helmholtz Association HGF, for the provision of beamline P02.2 at PETRA-III, allocated under proposal I-20221042. We are grateful to beamline scientists Nico Giordano, Konstantin Glazyrin and Hanns-Peter Liermann for their help during the experiments. The ESRF (Grenoble, France) is acknowledged for providing access to beamline ID15B for beamtimes HC-5918 and HC-6165 and ID27 for proposals HC-5909 and HC-5913. We thank beamline scientists Michael Hanfland, Gaston Garbarino, Samuel Gallego, Mohammed Mezouar, Anna Pakhomova and Bjorn Wehinger for their support. We also thank SPring-8 (Japan) for granting us access to the beamline BL10XU under the proposals 2024A1415 and 2024A1404. Beamline scientists Saori Kawaguchi and Hirokazu Kadobayashi are also acknowledge for their assistance. The Advance Photon Source (APS) at the Argonne National Laboratory (Chicago, USA) is acknowledged for allowing us to conduct our experiments at beamline 13 IDE-GSECARS for beamtime GUP-81704. We thank beamline scientists Vitali Prakapenka and Stella Chariton for their support during the experiments. Computational resources provided by the UK's National Supercomputer Service through the UK Car−Parrinello HEC Consortium (EP/X035891/1) and by the UK Materials and Molecular Modelling Hub (EP/P020194) are gratefully acknowledged.

■ REFERENCES

(1) Drozdov, A.; Kong, P.; Minkov, V.; Besedin, S.; Kuzovnikov, M.; Mozaffari, S.; Balicas, L.; Balakirev, F.; Graf, D.; Prakapenka, V. others Superconductivity at 250 K in lanthanum hydride under high pressures. *Nature* **2019**, *569*, 528−531.

(2) Drozdov, A.; Eremets, M.; Troyan, I.; Ksenofontov, V.; Shylin, S. I. Conventional superconductivity at 203 K at high pressures in the sulfur hydride system. *Nature* **2015**, *525*, 73−76.

(3) Hooper, J.; Altintas, B.; Shamp, A.; Zurek, E. Polyhydrides of the alkaline earth metals: a look at the extremes under pressure. *J. Phys. Chem. C* **2013**, *117*, 2982−2992.

(4) Hooper, J.; Zurek, E. High pressure potassium polyhydrides: a chemical perspective. *J. Phys. Chem. C* **2012**, *116*, 13322−13328.

(5) Baettig, P.; Zurek, E. Pressure-stabilized sodium polyhydrides: NaH_n ($n > 1$). *Phys. Rev. Lett.* **2011**, *106*, 237002.

(6) Shamp, A.; Hooper, J.; Zurek, E. Compressed cesium polyhydrides: Cs^+ sublattices and H^{3-}-three-connected nets. *Inorg. Chem.* **2012**, *51*, 9333−9342.

(7) Zurek, E.; Hoffmann, R.; Ashcroft, N.; Oganov, A. R.; Lyakhov, A. O. A little bit of lithium does a lot for hydrogen. *Proc. Natl. Acad. Sci. U. S. A.* **2009**, *106*, 17640−17643.

(8) Shipley, A. M.; Hutcheon, M. J.; Needs, R. J.; Pickard, C. J. High-throughput discovery of high-temperature conventional superconductors. *Phys. Rev. B* **2021**, *104*, 054501.

(9) Chen, C.-H.; Huang, A.; Tsuei, C.; Jeng, H.-T. Possible high-T_c superconductivity at 50 GPa in sodium hydride with clathrate structure. *New J. Phys.* **2021**, *23*, 093007.

(10) Pépin, C.; Loubeyre, P.; Occelli, F.; Dumas, P. Synthesis of lithium polyhydrides above 130 GPa at 300 K. *Proc. Natl. Acad. Sci. U. S. A.* **2015**, *112*, 7673−7676.

(11) Struzhkin, V. V.; Kim, D. Y.; Stavrou, E.; Muramatsu, T.; Mao, H.-k.; Pickard, C. J.; Needs, R. J.; Prakapenka, V. B.; Goncharov, A. F. Synthesis of sodium polyhydrides at high pressures. *Nat. Commun.* **2016**, *7*, 12267.

(12) Marqueño, T.; Kuzovnikov, M. A.; Osmond, I.; Dalladay-Simpson, P.; Hermann, A.; Howie, R. T.; Peña-Alvarez, M. High pressure study of sodium trihydride. *Front. Chem.* **2024**, *11*, 1306495.

(13) Ranieri, U.; Conway, L. J.; Donnelly, M.-E.; Hu, H.; Wang, M.; Dalladay-Simpson, P.; Peña Alvarez, M.; Gregoryanz, E.; Hermann, A.; Howie, R. T. Formation and Stability of Dense Methane-Hydrogen Compounds. *Phys. Rev. Lett.* **2022**, *128*, 215702.

(14) Zhou, D.; Semenok, D.; Galasso, M.; Alabarse, F. G.; Sannikov, D.; Troyan, I. A.; Nakamoto, Y.; Shimizu, K.; Oganov, A. R. Raisins in a hydrogen pie: Ultrastable cesium and rubidium polyhydrides. *Adv. Energy Mater.* **2024**, 2400077.

(15) Kuzovnikov, M. *Synthesis of novel rubidium superhydrides under high-pressure in 28th*. AIRAPT and 60th EHPRG International Conference, Edinburgh, 2023,.

(16) Peña-Alvarez, M.; Binns, J.; Marqués, M.; Kuzovnikov, M. A.; Dalladay-Simpson, P.; Pickard, C. J.; Ackland, G. J.; Gregoryanz, E.; Howie, R. T. Chemically assisted precompression of hydrogen molecules in alkaline-earth tetrahydrides. *J. Phys. Chem. Lett.* **2022**, *13*, 8447−8454.

(17) Marqués, M.; Peña-Alvarez, M.; Martínez-Canales, M.; Ackland, G. J. H2 chemical bond in a high-pressure crystalline environment. *J. Phys. Chem. C* **2023**, *127*, 15523−15532.

(18) Semenok, D. V.; Kruglov, I. A.; Savkin, I. A.; Kvashnin, A. G.; Oganov, A. R. On distribution of superconductivity in metal hydrides. *Curr. Opin. Solid State Mater. Sci.* **2020**, *24*, 100808.

(19) Zhao, W.; Song, H.; Liu, Z.; Du, M.; Zhang, Z.; Liu, Z.; Jiang, Q.; Chen, L.; Duan, D.; Cui, T. Pressure Induced Clathrate Hydrogen-Rich Superconductors KH_{20} and KH_{30}. *Inorg. Chem.* **2022**, *61*, 18112−18118.

(20) Hochheimer, H.; Strössner, K.; Hönle, W.; Baranowski, B.; Filipek, F. High pressure X-ray investigation of the alkali hydrides NaH, KH, RbH, and CsH. *Z. Phys. Chem.* **1985**, *143*, 139−144.

(21) Dorogokupets, P.; Dewaele, A. Equations of state of MgO, Au, Pt, NaCl-B1, and NaCl-B2: Internally consistent high-temperature pressure scales. *High Press. Res.* **2007**, *27*, 431−446.

(22) Howie, R. T.; Guillaume, C. L.; Scheler, T.; Goncharov, A. F.; Gregoryanz, E. Mixed molecular and atomic phase of dense hydrogen. *Phys. Rev. Lett.* **2012**, *108*, 125501.

(23) Birch, F. Finite elastic strain of cubic crystals. *Phys. Rev.* **1947**, *71*, 809.

(24) Ruff, S. W.; Christensen, P. R.; Barbera, P. W.; Anderson, D. L. Quantitative thermal emission spectroscopy of minerals: A laboratory technique for measurement and calibration. *J. Geophys. Res. Solid Earth* **1997**, *102*, 14899−14913.
(25) Joubert, J.-M. A Calphad-type equation of state for hydrogen gas and its application to the assessment of Rh−H system. *Int. J. Hydrogen Energy* **2010**, *35*, 2104−2111.
(26) Kuzovnikov, M. A.; Wang, B.; Wang, X.; Marqueño, T.; Shuttleworth, H. A.; Strain, C.; Gregoryanz, E.; Zurek, E.; Peña-Alvarez, M.; Howie, R. T. High Pressure Synthesis of Rubidium Superhydrides. *Phys. Rev. Lett.* **2025**, *134*, 196102.
(27) Bader, R. F. W. *Atoms in Molecules: A Quantum Theory*; Oxford University Press, 1994.
(28) Kuzovnikov, M. A.; Antonov, V. E.; Kulakov, V. I.; Usmanov, R. I. Heat capacity and other thermodynamic properties of hcp-CrH and hcp-CrD. *Int. J. Hydrogen Energy* **2025**, *116*, 507−515.
(29) Hwang, H. T.; Varma, A. Hydrogen storage for fuel cell vehicles. *Current Opin. Chem. Eng.* **2014**, *5*, 42−48.
(30) Coppola, C. M.; Tolbatov, I.; Tranca, I. C.; Coletti, C.; Marrone, A.; Storchi, L.; Profio, P. D.; Re, N.; Kazandjian, M. V.; Pellecchia, A. others A database approach for materials selection for hydrogen storage in aerospace technology. *Rendiconti Lincei* **2019**, *30*, 287−296.
(31) Ranieri, U.; Di Cataldo, S.; Rescigno, M.; Monacelli, L.; Gaal, R.; Santoro, M.; Andriambariarijaona, L.; Parisiades, P.; De Michele, C.; Bove, L. E. Observation of the most H_2-dense filled ice under high pressure. *Proc. Natl. Acad. Sci. U. S. A.* **2023**, *120*, No. e2312665120.
(32) Binns, J.; Dalladay-Simpson, P.; Wang, M.; Ackland, G. J.; Gregoryanz, E.; Howie, R. T. Formation of H_2-rich iodine-hydrogen compounds at high pressure. *Phys. Rev. B* **2018**, *97*, 024111.
(33) U.S. Department of Energy.; DOE Technical Targets for Onboard Hydrogen Storage. https://www.energy.gov/eere/fuelcells/doe-technical-targets-onboard-hydrogen-storage-light-duty-vehicles, Accessed: 2025−05−22.
(34) Chen, B.; Conway, L. J.; Sun, W.; Kuang, X.; Lu, C.; Hermann, A. Phase Stability and Superconductivity of Lead Hydrides at High Pressure. *Phys. Rev. B 103*, 035131.
(35) Liu, Z.; Li, J.; Zurek, E.; Zhuang, Q.; Liu, Y.; Yue, J.; Guo, S.; Zhang, A.; Chi, Z.; Huang, X.; Cui, T. Emergence of near Room-Temperature Superconductivity in Hydrides with H_2 Molecular Units. *Phys. Rev. B 109*, L180501.
(36) Guigue, B.; Loubeyre, P. No Observation of Lead Hydride in the Pb−H System under Pressure up to 140 GPa. *J. Appl. Phys. 129*, 225901.
(37) An, D.; Conway, L. J.; Duan, D.; Zhang, Z.; Jiang, Q.; Song, H.; Huo, Z.; Pickard, C. J.; Cui, T. Thermodynamically stable room-temperature superconductors in Li-Na hydrides under high pressures. *Adv. Funct. Mater.* **2025**, *35*, 2418692.
(38) Zhao, Y.; Zhang, X.; Li, X.; Ding, S.; Liu, Y.; Yang, G. Emergent superconductivity in K_2 ReH_9 under pressure. *J. Mater. Chem. C* **2022**, *10*, 14626−14632.
(39) He, X.-l.; Zhao, W.; Xie, Y.; Hermann, A.; Hemley, R. J.; Liu, H.; Ma, Y. Predicted Hot Superconductivity in $LaSc_2H_{24}$ under Pressure. *Proc. Natl. Acad. Sci. U. S. A. 121*, e2401840121.
(40) Li, S.; Wang, H.; Sun, W.; Lu, C.; Peng, F. Superconductivity in compressed ternary alkaline boron hydrides. *Phys. Rev. B* **2022**, *105*, 224107.
(41) Sun, W.; Chen, B.; Li, X.; Peng, F.; Hermann, A.; Lu, C. Ternary Na-PH superconductor under high pressure. *Phys. Rev. B* **2023**, *107*, 214511.
(42) Marqueño, T.; Osmond, I.; Kuzovnikov, M. A.; Shuttleworth, H. A.; Gallego-Parra, S.; Gregoryanz, E.; Hermann, A.; Howie, R. T.; Peña-Alvarez, M. Synthesis of Na_3WH_9 and Na_3ReH_8 Ternary Hydrides at High Pressures. *Inorg. Chem.* **2024**, *63*, 21734−21741.
(43) Spektor, K.; Crichton, W. A.; Filippov, S.; Simak, S. I.; Fischer, A.; Haussermann, U. Na3FeH7 and Na3CoH6: hydrogen-rich first-row transition metal hydrides from high pressure synthesis. *Inorg. Chem.* **2020**, *59*, 16467−16473.
(44) Spektor, K.; Kohlmann, H.; Druzhbin, D.; Crichton, W. A.; Bhat, S.; Simak, S. I.; Vekilova, O. Y.; Haussermann, U. Hypervalent hydridosilicate in the Na−Si−H system. *Front. Chem.* **2023**, *11*, 1251774.
(45) Muramatsu, T.; Wanene, W. K.; Somayazulu, M.; Vinitsky, E.; Chandra, D.; Strobel, T. A.; Struzhkin, V. V.; Hemley, R. J. Metallization and superconductivity in the hydrogen-rich ionic salt $BaReH_9$. *J. Phys. Chem. C* **2015**, *119*, 18007−18013.
(46) Meng, D.; Sakata, M.; Shimizu, K.; Iijima, Y.; Saitoh, H.; Sato, T.; Takagi, S.; Orimo, S.-i. Superconductivity of the hydrogen-rich metal hydride Li_5MoH_{11} under high pressure. *Phys. Rev. B* **2019**, *99*, 024508.

https://doi.org/10.1021/acs.jpclett.5c02024
J. Phys. Chem. Lett. 2025, 16, 9701−9707